

# Roles of polarization, phase and amplitude in solid immersion lens systems

Lars Egil Helseth

*University of Oslo, Department of Physics, N-0316 Oslo, Norway*

## Abstract

By altering the polarization, phase and amplitude at the exit pupil, the intensity distribution near the focal plane of a Solid Immersion Lens(SIL) system can be changed. We have studied how the resolution and focal depth changes for a few particular cases. It was seen that by impinging radial polarization on a SIL system, we may obtain a rotational symmetric z-component of the focused wavefront with spot size similar to that predicted by scalar theory. We also observed that it was possible to manipulate the contributions from the homogeneous and inhomogeneous waves behind the SIL by changing the amplitude and phase distribution at the aperture. In this way it may be possible to improve both the resolution and focal depth of the system.

## I. INTRODUCTION

The maximum resolution achievable with conventional optical techniques is determined by the classical diffraction limit. The minimum optical spot diameter can be expressed as  $\lambda/2NA$ , where  $\lambda$  is the wavelength in air, and  $NA = n\sin\alpha$  is the numerical aperture ( $n$  is the refractive index and  $\alpha$  is the convergence semiangle). Fortunately, the diffraction limit can be circumvented by use of scanning near-field optical systems, where resolutions less than 50nm can be achieved. Unfortunately, near-field techniques have been troubled by low transmission efficiencies, and therefore poor signal to noise ratios. Although recent research have improved the transmission efficiency considerably, it is still only 1% at 100nm spot size [1]. Another way to increase the resolution is by application of a Solid Immersion Lens(SIL) [2,3]. This method is currently not capable of the same resolution as the near-field techniques, but the light transmission efficiency is considerably better. The aim of the present paper is to describe how the polarization, phase and amplitude at the exit pupil influences the intensity distribution near the focal plane of a SIL. Although this is not a new issue in optics(see ref. [2–4] and references therein), we believe it is of interest to gain further understanding of SIL-systems as they may become an integral part of the future data storage systems. Since our focusing system has high NA and the focal point is placed many wavelengths away from the aperture, the diffracted field near the focal plane can be calculated using the Debye approximation [4,5]. Let us consider focusing through a dielectric interface(see fig. 1). The electric field inside medium  $i(= 1, 2)$  can be written as [4,5]:

$$\mathbf{E}_i = -\frac{ik_i}{2\pi} \int \int_{\Omega_i} \mathbf{T}(\mathbf{s}_i) \exp[ik_i(s_{ix}x + s_{iy}y + s_{iz}z)] ds_{ix} ds_{iy} \quad (1)$$

Where  $k_i = 2\pi n_i/\lambda_0$  is the wavenumber,  $\mathbf{s}_i = (s_{ix}, s_{iy}, s_{iz})$  is the unit vector along a typical ray,  $\Omega_i$  is the solid angle formed by all the geometrical rays,  $\mathbf{T}(\mathbf{s}_i)$  is the vector pupil distribution, which accounts for the polarization, phase and amplitude distribution at the exit pupil. We can find the electric field near the focal plane by matching the fields in the first and second medium at the interface,  $z = -d$ . The resulting electric field in the second medium becomes [5]:

$$\mathbf{E}_2 = C \int \int_{\Omega_1} \frac{\mathbf{T}(s_{1x}, s_{1y})}{s_{1z}} \exp[id(k_2 s_{2z} - k_1 s_{1z})] \exp[ik_2 s_{2z} z] \exp[ik_1(s_{1x}x + s_{1y}y)] ds_{1x} ds_{1y} \quad (2)$$

$C$  is a complex constant(which will be ignored in the rest of this paper). The unit wave-vector is defined in spherical coordinates:

$$\mathbf{s}_i = [\sin(\theta_i)\cos(\phi), \sin(\theta_i)\sin(\phi), \cos(\theta_i)] \quad (3)$$

The position vector can be written as(see also fig. 1):

$$\mathbf{r}_c = r_c[\sin(\theta_c)\cos(\phi_c), \sin(\theta_c)\sin(\phi_c), \cos(\theta_c)] \quad (4)$$

This gives the following diffraction integral:

$$\mathbf{E}_2 = \int_0^\alpha \int_0^{2\pi} \mathbf{T}(\theta_1, \phi) \exp[ik_0(r_c\kappa + \Psi)] \sin(\theta_1) d\theta_1 d\phi \quad (5)$$

$$\mathbf{T}(\theta_1, \phi) = \mathbf{P}(\theta_1, \phi)A(\theta_1, \phi) \quad (6)$$

where  $\alpha$  is the convergence semiangle,  $\mathbf{P}(\theta_1, \phi)$  is the polarization and  $A(\theta_1, \phi)$  represents the amplitude and phase distribution at the exit pupil. We will for the rest of this paper assume that our optical system obeys the sine condition,  $A(\theta_1) \propto \sqrt{\cos(\theta_1)}$ , see e.g. ref. [4,5].

$$\kappa = n_2 \cos(\theta_2) \cos(\theta_c) + n_1 \sin(\theta_1) \sin(\theta_c) \cos(\phi - \phi_c) \quad (7)$$

and

$$\Psi = d[n_2 \cos(\theta_2) - n_1 \cos(\theta_1)] \quad (8)$$

$\Psi$  represents the aberration function introduced due to the mismatch in refractive index. A detailed derivation of this integral was first presented in reference [5]. We have presented it in a slightly different form to enlight the further discussion in this paper. We will consider two particular cases: 1) Focusing of electromagnetic waves in a homogeneous media (air). In this case  $n_1 = n_2 = 1$ . 2) Focusing of electromagnetic waves with a SIL, which means that  $d=0$  (note that  $n_1 > n_2$ ). In both cases the aberration function  $\Psi$  is identically zero [6].

## II. THE INFLUENCE OF POLARIZATION

The state of the polarization incident on the focusing system will influence the resolution near the focal plane (see e.g. [4,7]). To discuss this question quantitatively, we must find a general expression for the polarization vector. We assume a incident polarization which may in general depend on the polar and azimuthal angle:

$$\mathbf{P}_0 = \begin{bmatrix} a(\theta_1, \phi) \\ b(\theta_1, \phi) \\ 0 \end{bmatrix}$$

The polarization vector can be written as [5]:

$$\mathbf{P}(\theta_1, \phi) = \mathbf{R}^{-1}[\mathbf{L}^{(2)}]^{-1} \mathbf{I} \mathbf{L}^{(1)} \mathbf{C} \mathbf{R} \mathbf{P}_0 \quad (9)$$

$$\mathbf{R} = \begin{bmatrix} \cos(\phi) & \sin(\phi) & 0 \\ -\sin(\phi) & \cos(\phi) & 0 \\ 0 & 0 & 1 \end{bmatrix}$$

which describes the rotation of the co-ordinate system around the optical axis;

$$\mathbf{C} = \begin{bmatrix} \cos(\theta_1) & 0 & \sin(\theta_1) \\ 0 & 1 & 0 \\ -\sin(\theta_1) & 0 & \cos(\theta_1) \end{bmatrix}$$

which describes the change of polarization on propagation through the lens;

$$\mathbf{L}^{(j)} = \begin{bmatrix} \cos(\theta_j) & 0 & -\sin(\theta_j) \\ 0 & 1 & 0 \\ \sin(\theta_j) & 0 & \cos(\theta_j) \end{bmatrix}$$

which describes a rotation of the co-ordinate system into s and p-polarized vectors;

$$\mathbf{I} = \begin{bmatrix} t_p & 0 & 0 \\ 0 & t_s & 0 \\ 0 & 0 & t_p \end{bmatrix}$$

which represents the transmission(Fresnel coefficients) through the plane dielectric interface.

This results in:

$$\mathbf{P}(\theta_1, \phi) = \begin{bmatrix} a[t_p \cos(\theta_2) \cos^2(\phi) + t_s \sin^2(\phi)] + b[t_p \cos(\theta_2) \sin(\phi) \cos(\phi) - t_s \sin(\phi) \cos(\phi)] \\ a[t_p \cos(\theta_2) \cos(\phi) \sin(\phi) - t_s \sin(\phi) \cos(\phi)] + b[t_p \cos(\theta_2) \sin^2(\phi) + t_s \cos^2(\phi)] \\ -at_p \sin(\theta_2) \cos(\phi) - bt_p \sin(\theta_2) \sin(\phi) \end{bmatrix}$$

In the special case of x-polarized incident light( $a = 1$  and  $b=0$ ) this matrix reduces to [5];

$$\mathbf{P}(\theta_1, \phi) = \begin{bmatrix} \frac{1}{2}(t_p \cos(\theta_2) + t_s) + \frac{1}{2}(t_p \cos(\theta_2) - t_s) \cos(2\phi) \\ \frac{1}{2}(t_p \cos(\theta_2) - t_s) \sin(2\phi) \\ -t_p \sin(\theta_2) \cos(\phi) \end{bmatrix}$$

It is seen that different angles have different amplitudes, and that the polarization is dependent on  $\phi$ . Another possibility was explored by Quabis et. al. [8], who found that radial polarized light may increase the resolution. We extend their analysis to a SIL system. We may write  $a(\phi) = \cos\phi$  and  $b(\phi) = \sin\phi$ :

$$\mathbf{P}(\theta_1, \phi) = \begin{bmatrix} t_p \cos(\theta_2) \cos(\phi) \\ t_p \cos(\theta_2) \sin(\phi) \\ -t_p \sin(\theta_2) \end{bmatrix}$$

When inserted in eq. (5), this gives:

$$E_{2x} = iI_1^{rad} \cos(\phi_c) \quad (10)$$

$$E_{2y} = iI_1^{rad} \sin(\phi_c) \quad (11)$$

$$E_{2z} = -I_0^{rad} \quad (12)$$

$$I_0^{rad} = \int_0^\alpha B(\theta_1) t_p \sin(\theta_2) \sin(\theta_1) J_0(k_1 r_c \sin(\theta_1) \sin(\theta_c)) \exp(ik_0 \Psi) \exp(ik_2 z \cos(\theta_2)) d\theta_1 \quad (13)$$

$$I_1^{rad} = \int_0^\alpha B(\theta_1) t_p \cos(\theta_2) \sin(\theta_1) J_1(k_1 r_c \sin(\theta_1) \sin(\theta_c)) \exp(ik_0 \Psi) \exp(ik_2 z \cos(\theta_2)) d\theta_1 \quad (14)$$

where  $B(\theta_1) = \sqrt{\cos(\theta_1)}$ , and  $J_n$  is the Bessel function of the first kind, of order  $n$ . The z-component is completely independent of the azimuthal angle, and its importance increases

with increasing NA. Let us assume that we are able to find a medium which is only sensitive to the z-component of the polarization. That is, we may use the z-component, and disregard the x and y-components. Fig. 2 shows the energy density at the bottom surface(the focal plane) of a SIL with  $n_1 = 2$ (and  $n_2 = 1$ ), for both radial(solid line) and x-polarized incident light(the dashed line represents  $\phi_c = 0^\circ$ , whereas the dotted line represents  $\phi_c = 90^\circ$ ). In this example, we assume that  $\alpha = 60^\circ$  and the wavelength  $\lambda_0 = 635nm$ . Fig. 2 indicates that it is possible to increase the resolution, and perhaps reproduce the result predicted by scalar theory. However, it is worth noting that in practice one must combine the radial polarizer in front of the focusing system with an annular aperture, both to increase resolution and to avoid a singularity on the axis. This was discussed by Quabis et. al. [8]. Therefore, if one could find a material which is sensitive only to the z-component, a more detailed calculation using an annular aperture is required to determine the real resolution.

### III. THE INFLUENCE OF AMPLITUDE AND PHASE

The spatial amplitude and phase distribution(at the exit pupil) will also influence the energy distribution near the focal plane(see e.g. [4,7,9]). As with the incident polarization, there are countless ways to alter the phase and transmittance. We will limit our discussion to the special class of amplitude/phase filters called annular apertures(see ref. [10,11] and references therein). Annular apertures that modifies the transmittance and/or phase distribution at the exit pupil may improve the resolution at the expense of higher sidelobes. In this section we will discuss the effect of such an aperture in front of a focusing system containing a SIL. The transmittance through an annular aperture can be expressed as:

$$A(\theta_1) = B(\theta_1) \begin{cases} T_1 & \text{if } 0 < \theta_1 < \alpha_1 \\ T_2 & \text{if } \alpha_1 < \theta_1 < \alpha_2 \\ \vdots & \\ T_i & \text{if } \alpha_{i-1} < \theta_1 < \alpha_i \\ \vdots & \\ T_N & \text{if } \alpha_{N-1} < \theta_1 < \alpha_N \end{cases}$$

where  $T_i$  are complex constants(phase and amplitude) for the various zones in the aperture, and  $B(\theta_1) = \sqrt{\cos(\theta_1)}$ . If the incident light is polarized in the x-direction(a=1, b=0), the resulting field can be found by inserting the transmittance into eq. (5):

$$E_{2x} = i[I_0 + I_2 \cos(2\phi_c)] \quad (15)$$

$$E_{2y} = iI_2 \sin(2\phi_c) \quad (16)$$

$$E_{2z} = 2I_1 \cos(\phi_c) \quad (17)$$

where

$$I_0 = \sum_{i=1}^N (T_i - T_{i+1}) \int_0^{\alpha_i} A^{0x}(\theta_1) J_0(k_1 r_c \sin(\theta_1) \sin(\theta_c)) \exp(ik_0 \Psi) \exp(ik_2 z \cos(\theta_2)) d\theta_1 \quad (18)$$

$$I_1 = \sum_{i=1}^N (T_i - T_{i+1}) \int_0^{\alpha_i} A^{1x}(\theta_1) J_1(k_1 r_c \sin(\theta_1) \sin(\theta_c)) \exp(ik_0 \Psi) \exp(ik_2 z \cos(\theta_2)) d\theta_1 \quad (19)$$

$$I_2 = \sum_{i=1}^N (T_i - T_{i+1}) \int_0^{\alpha_i} A^{2x}(\theta_1) J_2(k_1 r_c \sin(\theta_1) \sin(\theta_c)) \exp(ik_0 \Psi) \exp(ik_2 z \cos(\theta_2)) d\theta_1 \quad (20)$$

$$A^{0x} = B(\theta_1)(t_s + t_p \cos(\theta_2)) \sin(\theta_1) \quad (21)$$

$$A^{1x} = B(\theta_1) t_p \sin(\theta_2) \sin(\theta_1) \quad (22)$$

$$A^{2x} = B(\theta_1)(t_s - t_p \cos(\theta_2)) \sin(\theta_1) \quad (23)$$

Where  $T_{N+1}$  is defined to be zero, and we have used that  $\int_{\alpha_i}^{\alpha_{i+1}} = \int_0^{\alpha_{i+1}} - \int_0^{\alpha_i}$  to derive these equations. Similar expressions can be applied to the case of radial polarized light. From eqs. (18), (19) and (20) we can see that the total field is a sum of electric fields from zones with increasing angular extent, and we expect that the terms with the smallest  $\alpha_i$  must be carefully balanced against each other in order to reduce the energy in the sidelobes. For high NA systems, the z-component becomes particularly important, and may increase the sidelobe intensity substantially. Thus it is necessary to keep the center peak ratio high in order to avoid a dominating z-component, which may increase the the sidelobes as well as the spot size. In total one must not only balance the terms from the various zones, both also keep the sidelobes due to the z-(and y)component at an acceptable level. This is a difficult task, and is best treated by numerical analysis, e.g. by binary search methods [11]. To keep the physics simple, we will limit ourselves to apertures with two and three zones. The profiles (the time-averaged energy density distributions) will be normalized, for simple comparison between systems.

### A. Focusing in a homogenous media

In order to compare with the situations occurring in a SIL-system, we first observe what happens when we place a three-zone aperture in front of a system focusing in a homogeneous media. As pointed out by Ando [10], the center-peak intensity ratio can be maximized by using a phase aperture, and the sidelobes can be made small by maintaining the same phase for the light passing through the center and outer portion of the aperture. On the basis of these results, let us assume that  $T_1 = 1$ ,  $T_2 = -1$  and  $T_3 = 1$ . Such an aperture can be produced by e.g. lithographical methods, and was experimentally tested by Ando et. al. [12]. Let  $\alpha_1 = 15^\circ$ ,  $\alpha_2 = 30^\circ$ ,  $\alpha_3 = 60^\circ$  and  $\lambda_0 = 635nm$ . Fig. 3 shows the focused beam profile for the three-zone phase aperture when  $\phi_c = 0^\circ$  (solid line) and  $\phi_c = 90^\circ$  (dash-dotted line). For comparison we have also plotted the profile of the focused beam with no aperture when  $\phi_c = 0^\circ$  (dashed line) and  $\phi_c = 90^\circ$  (dotted line). The resolution due to the three-zone aperture is improved as compared to no aperture, but the peak sidelobe intensity is almost 20%. We could probably bring this number down by increasing the number of zones in the annular aperture. Fig. 4 shows the axial energy density distribution for the three-zone annular aperture (solid line) and no annular aperture (dashed line). Note that the focal depth is larger with the three-zone aperture.

## B. Focusing with a SIL

The last ten years much research has been done on SIL systems [2,3,13–15]. As mentioned in the introduction, a major goal has been to improve the resolution and focal depth. To that end, an interesting possibility is the application of an annular aperture in front of a SIL. As have been pointed out by Milster *et al* [3], plane waves incident on the bottom surface of the SIL will experience total reflection above the critical angle,  $\theta_c = \arcsin(n_2/n_1)$ . Thus we may divide the plane waves at the exit pupil into two parts; a homogeneous part where the angles are smaller than the critical angle at the interface, and an inhomogeneous part where the plane waves experience total reflection at the interface, corresponding to evanescent waves below the bottom surface of the SIL. Let us first see what happens when we put a simple two-zone annular aperture with  $T_1 = 0$  and  $T_2 = 1$  in front of the SIL. The dotted lines in figs. 5 and 6 show the transverse profiles behind the bottom surface of the SIL ( $n_1 = 2.0$ ,  $n_2 = 1.0$  and  $\lambda_0 = 635nm$ ) when  $\phi_c = 0^\circ$  and  $\phi_c = 90^\circ$ , respectively. We assume that  $\alpha_1 = 54^\circ$  and  $\alpha_2 = 60^\circ$ . For comparison, the profiles for a SIL with no annular aperture are also shown (the dashed lines in figs. 5 and 6). Note that as the center (dark) disk increases, the profile becomes more compressed, but the sidelobes increases. The increase in resolution is more pronounced when  $\phi_c = 90^\circ$  than  $\phi_c = 0^\circ$ , since the z-component of the electric field depends on  $\cos\phi_c$  (which is zero when  $\phi_c = 90^\circ$ , see eq. (17)). Fig. 7 shows the axial distribution behind the SIL with (dotted line) or without (dashed line) a two-zone annular aperture. When the center disk increases, the focal depth decreases, contrary to what happens during focusing in a homogeneous media [9]. This behaviour occur since the evanescent waves becomes more dominating when we block out the homogeneous waves, and since the amplitude of evanescent waves are decreasing exponentially behind the SIL. To increase the light transmission efficiency, one may replace the two-zone amplitude aperture with an axicon, thus creating a bright ring.

Next we place a three-zone phase aperture (with the same properties as in the previous section) in front of the SIL. In particular, we are interested in observing what happens when 1)  $\alpha_1 < \alpha_2 \leq \theta_c$  and 2)  $\alpha_2 > \alpha_1 \geq \theta_c$ . The first case ( $\alpha_1 < \alpha_2 \leq \theta_c$ ) is in some ways similar to focusing in a homogeneous media. That is, we expect the spot size to decrease, if the convergence semiangles have proper values. However, we also expect the focal depth to decrease, since we balance terms with homogeneous waves against each other, thus increasing the importance of the evanescent waves. As an example, let us consider the same SIL-system as above, but now replace the two-zone aperture with a three-zone annular aperture with  $\alpha_1 = 20^\circ$ ,  $\alpha_2 = 30^\circ$  and  $\alpha_3 = 60^\circ$ . The dash-dotted lines in figs. 5 and 6 shows the resulting profiles when  $\phi_c = 0^\circ$  and  $\phi_c = 90^\circ$ , respectively. Note that the profile is slightly smaller than the dashed line (no annular aperture) when  $\phi_c = 90^\circ$ , whereas for  $\phi_c = 0^\circ$  it is slightly larger. The dash-dotted line in fig. 7 shows the axial distribution. As expected, the focal depth is smaller with the annular aperture.

In the second case ( $\alpha_2 > \alpha_1 \geq \theta_c$ ) the opposite behaviour may take place. That is, we are able to balance terms with inhomogeneous waves against each other, thus increasing the importance of the homogeneous waves. In this way we can produce some kind of enhancement of the focal depth, and if the the angles  $\alpha_1$  and  $\alpha_2$  are properly chosen, the beam profile may become narrower as well. As an example we consider an annular aperture with  $\alpha_1 = 31^\circ$  and  $\alpha_2 = 43^\circ$ . The solid lines in figs. 5 and 6 are representing the transverse profiles when

$\phi_c = 0^\circ$  and  $\phi_c = 90^\circ$ , respectively. Now the situation is almost opposite compared with the previous annular aperture. That is, the profile is smaller than the dashed line(no aperture) when  $\phi_c = 0^\circ$ , but larger when  $\phi_c = 90^\circ$ . The axial distribution(solid line in fig. 7) is decaying more slowly than with no annular aperture, which confirms the discussion above.

#### IV. CONCLUSION

The choice of incident polarization, phase and amplitude may change the intensity distribution near the focal plane of a focusing system. It was seen that by impinging radial polarization on a SIL system, we may obtain a rotational symmetric z-component of the focused wavefront with spot size similar to that predicted by scalar theory. We also discussed how annular apertures may change the resolution and focal depth. It was shown that when we place a three-zone phase aperture in front of a focusing system, both the resolution and focal depth may increase. When applied to SIL-systems, we observed that it was possible to manipulate the contributions from the homogeneous and inhomogeneous waves behind the SIL by changing the phase and transmittance distribution at the aperture. In this way it may be possible to improve both the resolution and focal depth. Future investigations may be directed towards the use of more than three zones to improve the resolution and focal depth. We would like to point out that only a few special cases were discussed in this paper, and that our examples were not optimized for any particular applications.

#### ACKNOWLEDGMENTS

I would like to thank all the people working in the Superconductivity and Magneto-optics group at the University of Oslo for creating a very active and inspiring environment, which resulted in the ideas presented in this work. The research was financially supported by The Norwegian Research Council.

## REFERENCES

- [1] P.N.Minh, T.Ono: *Rev. Sci. Instr.*, 71 (2000), 3111.
- [2] I.Ichimura, S.Hayashi, G.S.Kino: *Appl. Opt.*, 36(1997), 4339.
- [3] T.D.Milster, J.S.Jo, K.Hirota: *Appl. Opt.* , 38 (1999), 5046.
- [4] J.J.Stamnes *Waves in focal regions* 1st ed.(Adam Hilger, Bristol, UK, 1986)
- [5] P.Török, P.Varga, Z.Laczik and G.R.Booker: *J. Opt. Soc. Am. A* 12(1995), 325.
- [6] P.Török, C.J.R.Sheppard, P.Varga: *J. Mod. Opt.* 43(1996), 1167.
- [7] C.J.R.Sheppard, K.G.Larkin: *J. Mod. Opt.* 41(1994), 1495.
- [8] S.Quabis, R.Dorn, M.Eberler, O.G. Glöckl, G.Leuchs: *Opt. Commun.*, 179 (2000), 1.
- [9] T.C.Poon, M.Motamedi: *Appl. Opt.*, 26 (1987), 4612.
- [10] H.Ando: *Jpn. J. Appl. Phys.* ,31 (1992), 557.
- [11] G.Yang: *Opt. Commun.*, 159 (1999), 19.
- [12] H.Ando, T.Yokota, K.Tanoue: *Jpn. J. Appl. Phys.* ,32 (1993), 5269.
- [13] S.Hasegawa, N.Aoyama, A.Futamata, T.Uchiyama: *Appl. Opt.* ,38 (1999), 2297.
- [14] F.Guo, T.E.Schlesinger, D.D.Stancil: *Appl. Opt.* ,39 (2000), 324.
- [15] K.Shimura, T.D.Milster, J.S.Jo, K.Hirota: *Jpn. J. Appl. Phys.* ,39 (2000), 897.

## FIGURES

FIG. 1. The general geometry for focusing through a planar dielectric interface, located at  $z=-d$ . The focal plane is located at  $z=0$ .

FIG. 2. The transversal time-averaged electric energy density when  $n_1 = 2$ ,  $n_2 = 1$  and  $\alpha = 60^\circ$ . 1)z-component of the radial polarized focused beam. 2)Total energy density for incident x-polarized light( $a=1$  and  $b=0$ ) when  $\phi_c = 0^\circ$ . 3)Total energy density for incident x-polarized light( $a=1$  and  $b=0$ ) when  $\phi_c = 90^\circ$ .

FIG. 3. The transversal time-averaged electric energy density with and without a three-zone annular aperture( $\alpha_1 = 15^\circ$  and  $\alpha_2 = 30^\circ$ ) when  $n_1 = n_2 = 1$  and  $\alpha = 60^\circ$ . 1)Three-zone annular aperture when  $\phi_c = 0^\circ$  2)No annular aperture when  $\phi_c = 0^\circ$ . 3)No annular aperture when  $\phi_c = 90^\circ$ . 4)Three-zone annular aperture when  $\phi_c = 90^\circ$

FIG. 4. The axial time-averaged electric energy density when  $n_1 = n_2 = 1$  and  $\alpha = \alpha_3 = 60^\circ$ . 1)Three-zone annular aperture with  $\alpha_1 = 15^\circ$  and  $\alpha_2 = 30^\circ$ . 2)No annular aperture.

FIG. 5. The transversal time-averaged electric energy density when  $\phi_c = 0^\circ$ ,  $n_1 = 2$ ,  $n_2 = 1$  and  $\alpha = \alpha_3 = 60^\circ$ . 1)Three-zone phase aperture with  $\alpha_1 = 31^\circ$  and  $\alpha_2 = 43^\circ$ . 2)No annular aperture. 3)Two-zone annular aperture with  $\alpha_1 = 54^\circ$ . 4)Three-zone aperture with  $\alpha_1 = 20^\circ$  and  $\alpha_2 = 30^\circ$ .

FIG. 6. The transversal time-averaged electric energy density when  $\phi_c = 90^\circ$ ,  $n_1 = 2$ ,  $n_2 = 1$  and  $\alpha = \alpha_3 = 60^\circ$ . 1)Three-zone phase aperture with  $\alpha_1 = 31^\circ$  and  $\alpha_2 = 43^\circ$ . 2)No annular aperture. 3)Two-zone annular aperture with  $\alpha_1 = 54^\circ$ . 4)Three-zone aperture with  $\alpha_1 = 20^\circ$  and  $\alpha_2 = 30^\circ$ .

FIG. 7. The axial time-averaged electric energy density when  $n_1 = 2$ ,  $n_2 = 1$  and  $\alpha = \alpha_3 = 60^\circ$ . 1)Three-zone phase aperture with  $\alpha_1 = 31^\circ$  and  $\alpha_2 = 43^\circ$ . 2)No annular aperture. 3)Two-zone annular aperture with  $\alpha_1 = 54^\circ$ . 4)Three-zone aperture with  $\alpha_1 = 20^\circ$  and  $\alpha_2 = 30^\circ$ .

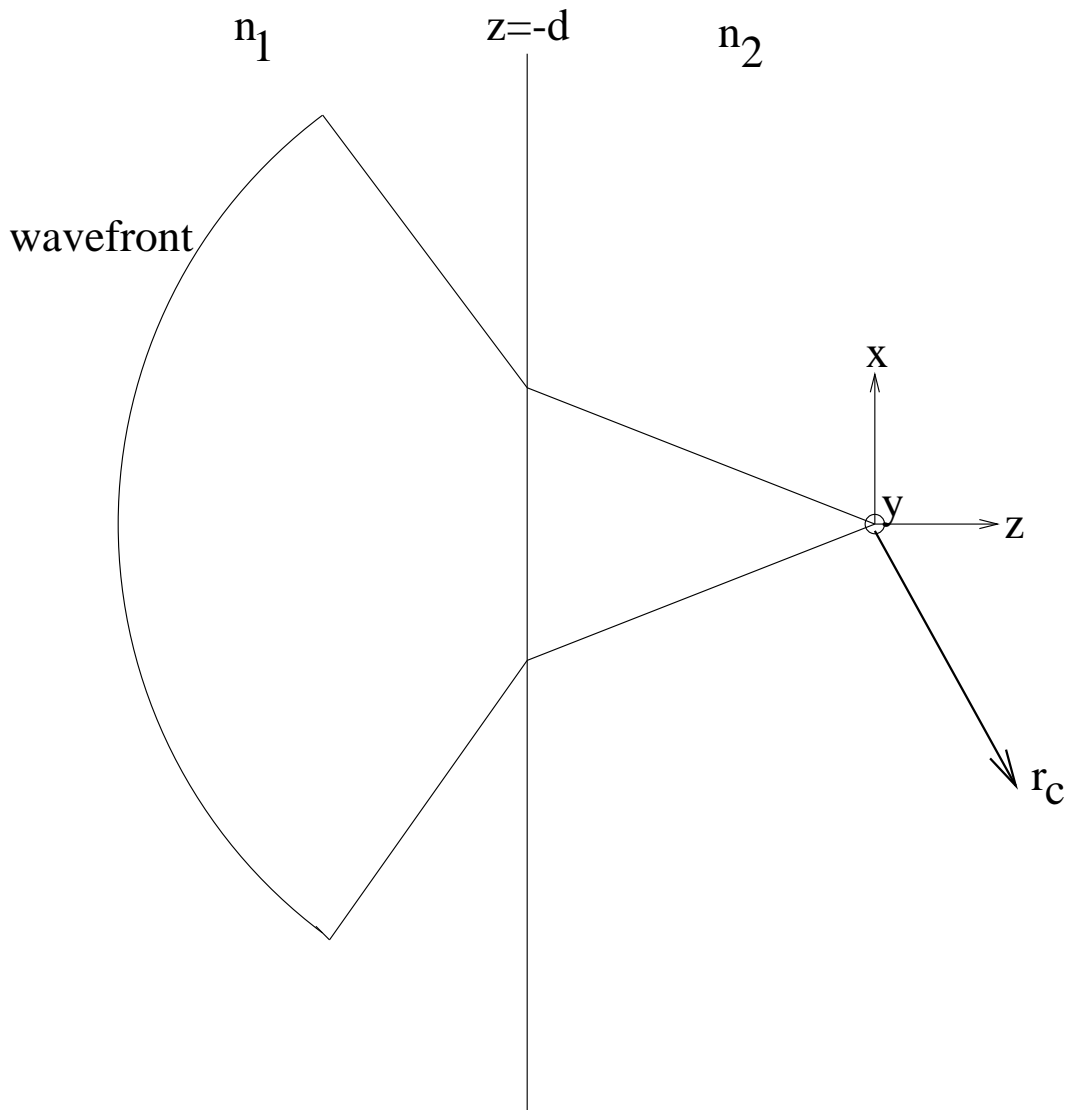


Figure 1

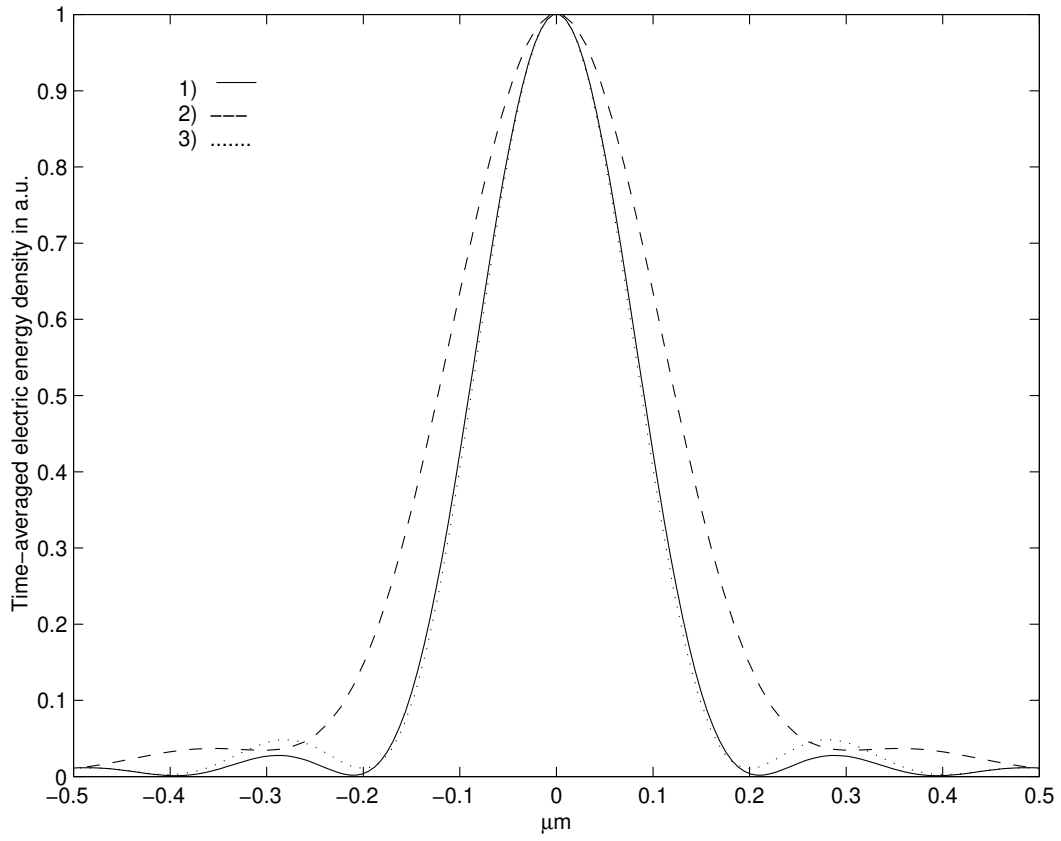


Figure 2

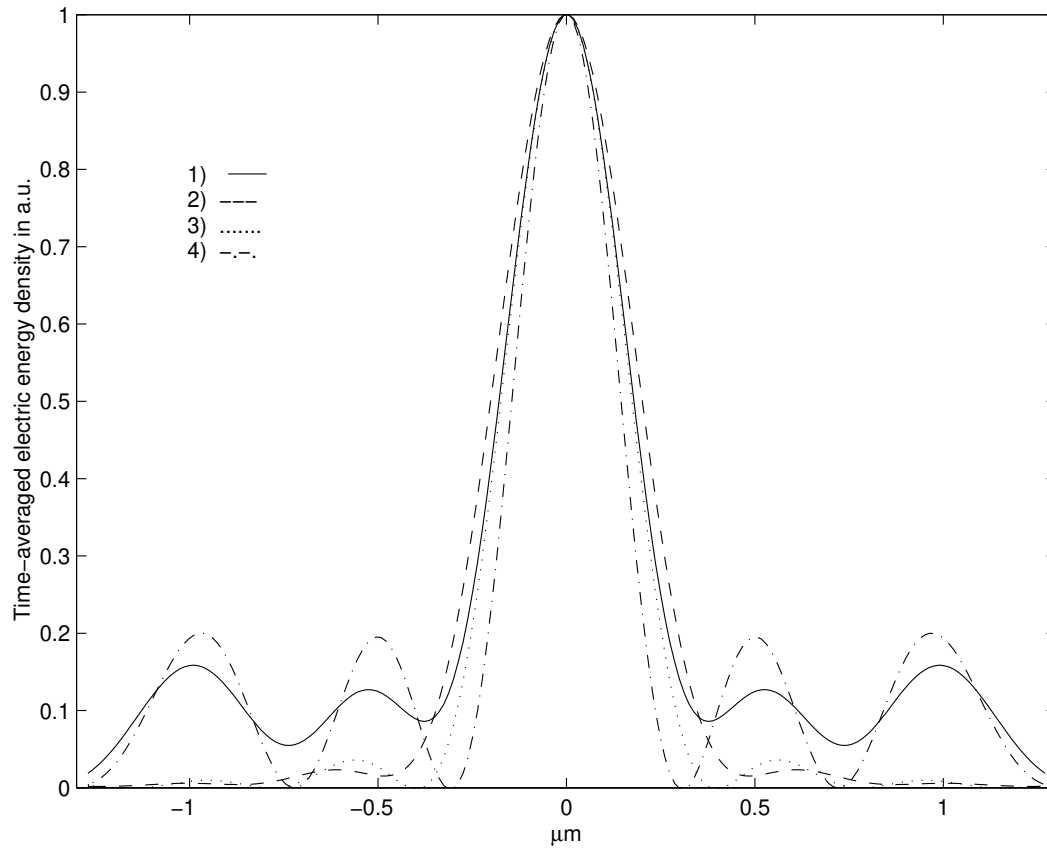


Figure 3

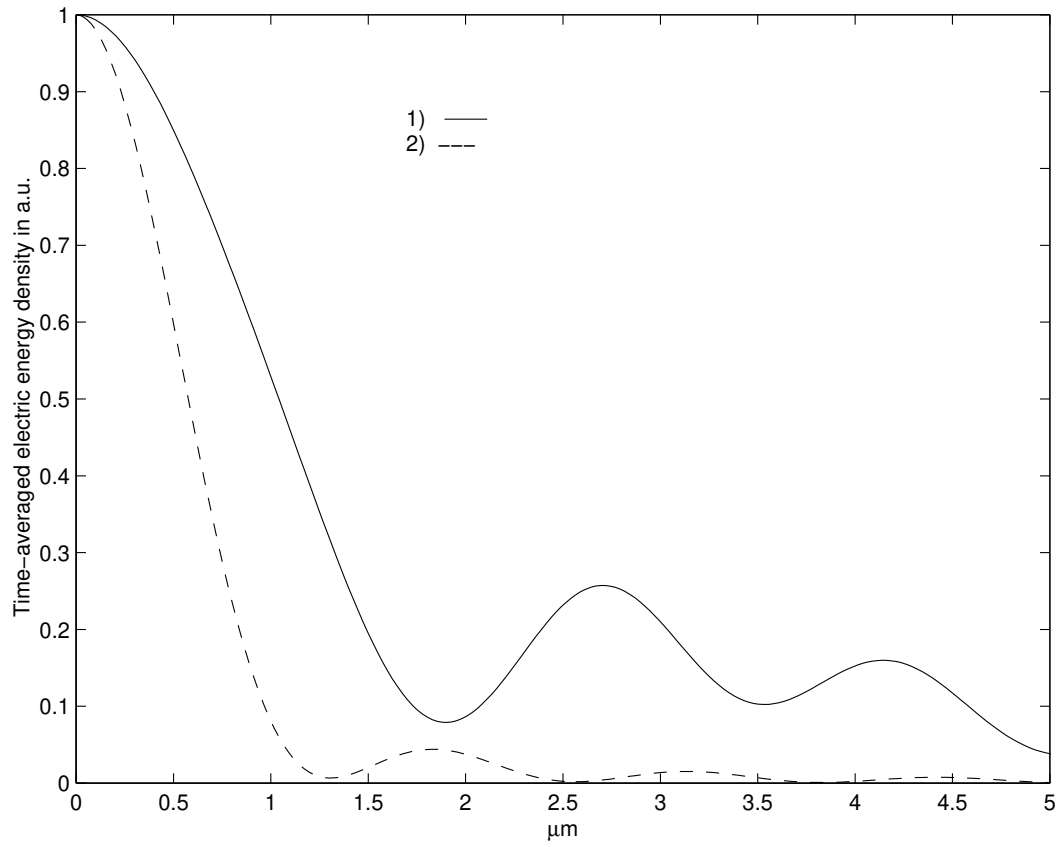


Figure 4

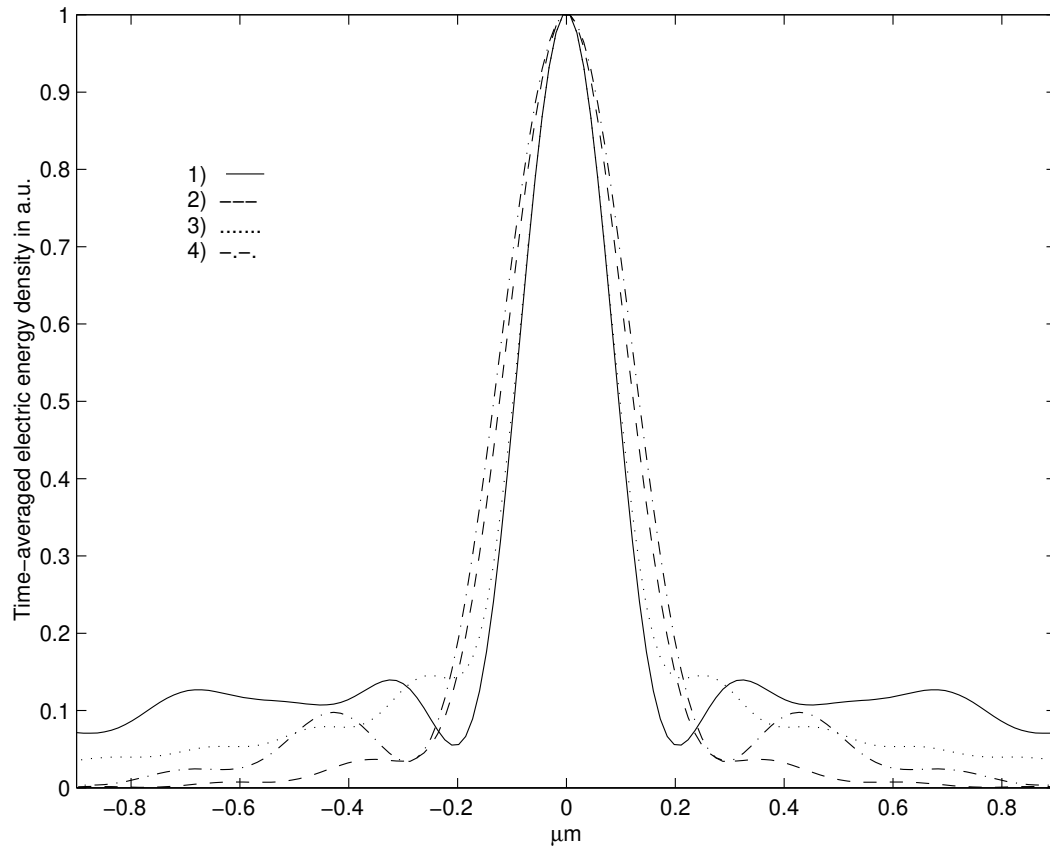


Figure 5

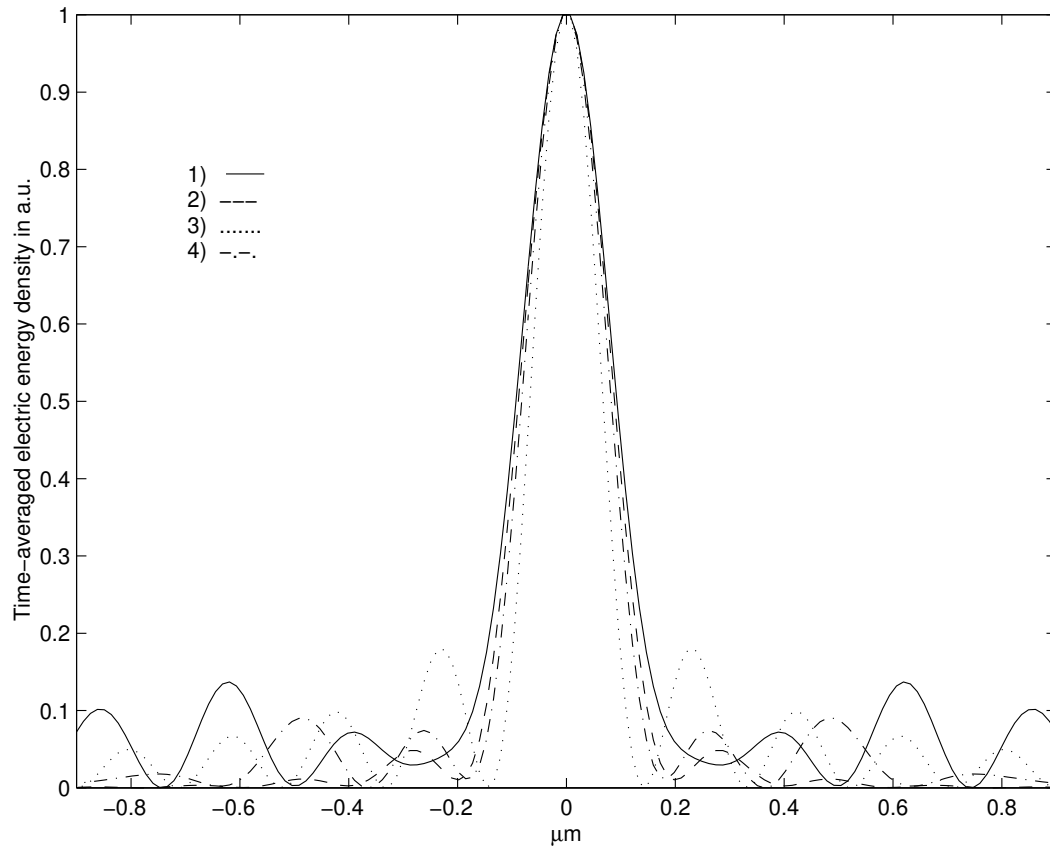


Figure 6

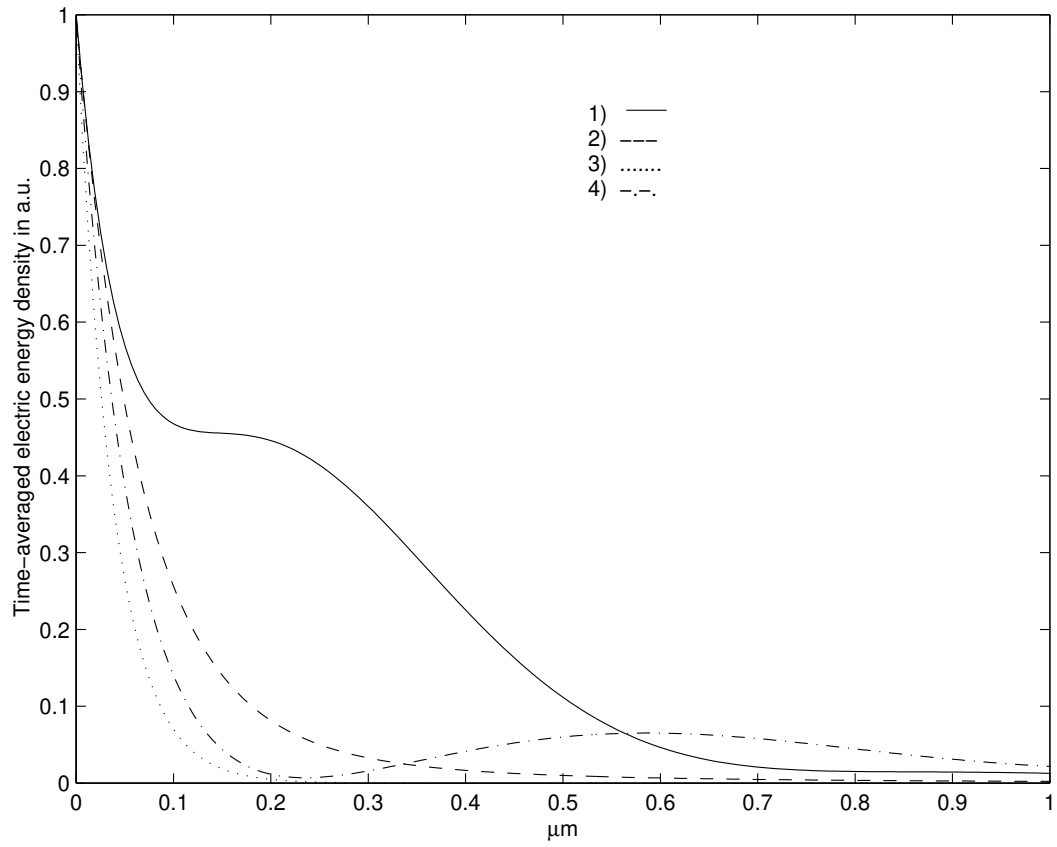


Figure 7